Journal of Thermal Engineering, Vol. 5, No. 4, pp. 355-371, July, 2019
Yildiz Technical University Press, Istanbul, Turkey

ENERGY AND EXERGY ANALYSIS OF A VAPOR ABSORPTION REFRIGERATION SYSTEM IN AN INTERCITY BUS APPLICATION

N. Kurtulmuş[1,*], M. Bilgili[2], B. Şahin[3]

ABSTRACT

A Vapor Absorption Refrigeration (VAR) system driven by the exhaust gas waste heat received from the internal combustion engine of an intercity bus is modeled and analyzed for air-conditioning the intercity bus cabin under different operating parameters. Initially, the hourly comfort cooling load of the intercity bus is calculated for a cooling season spanning five months between May and October in Turkey. After determining the capacity of heat source sufficiency for air-conditioning the intercity bus, energy and exergy analyses of the VAR system are conducted, then designed and compared with the vapor compression refrigeration system in respect to the effect of fuel consumption. The results show that approximately 4,489 kg/year of fuel can be saved by using the VAR system driven by an exhaust gas waste heat in an intercity bus. The maximum coefficient of performance (COP) of the VAR system is obtained as 0.78 at 5 a.m. in May, and the maximum total exergy destruction for the VAR system is obtained as 15.25 kW at 4 p.m. in July. Lastly, the specific time is selected to investigate the effect of operating and environmental parameters on the VAR system.

Keywords: *Energy, Exergy, Intercity Bus Air-Conditioning, Vapor Absorption Refrigeration System, Water-Lithium Bromide*

INTRODUCTION

A large amount of waste heat is released to the ambient from the internal combustion engines in the automotive industry. There are several methods to utilize waste heat to meet the energy requirement of a refrigeration or air- conditioning process. Air-conditioning of the cabin, especially for vehicles with large cabins such as intercity buses, requires considerable mechanical energy input, ranging from 5 kW to10 kW. One of the methods that is suitable in terms of energy efficiency and economic feasibility is to utilize the waste heat of exhaust gas for the implementation of Vapor Absorption Refrigeration (VAR). The VAR system provides the required cooling by the evaporator component, which is also the case for a Vapor Compression Refrigeration (VCR) system. The VAR system requires heat energy to be driven because there is a physico-chemical process in the cycle, whereas a VCR system requires mechanical energy to drive the system. Commercial VAR systems generally use two different working solutions—ammonia-water (ammonia is refrigerant) and water-LiBr (water is refrigerant). While the VAR system using ammonia-water is preferred for refrigeration processes requiring low temperatures, the VAR system using water-LiBr is preferred for air-conditioning applications [1-4].

Several methods were applied for recovering waste heat from exhaust gases of the internal combustion engines [5, 6]. The researchers claimed that utilizing exhaust gas waste heat received from engines in the VAR systems could be an alternative for cooling applications [7, 8]. When using the VAR system driven by waste heat of exhaust gas, some applications require low temperature refrigeration such as the truck refrigeration system used for preserving the perishable food during the transportation. Koehler et al. [9] investigated a VAR system driven by waste heat received from the exhaust gases for truck refrigeration. For that refrigeration purpose, they designed and constructed a prototype of an absorption refrigeration system and finally tested it under various operational conditions. The system was also evaluated at different cases including city traffic, mountains and plain road. The results of their investigations indicated that the COP value of the prototype was around 0.27, which could be improved beyond that value, and that the system could be an alternative for long-distance plain road transportation. Another experimental research work were conducted on the application of a low-temperature refrigeration system by Horuz [10], who aimed to investigate the performance of a VAR system driven by waste heat received from exhaust gases under different conditions. Many other researchers [11, 12] studied VAR

This paper was recommended for publication in revised form by Regional Editor Tolga Taner
[1]Adana Science and Technology University, Faculty of Engineering and Natural Science, Mech. Eng. Dept., Adana/Turkey
[2]Cukurova University, Ceyhan Engineering Faculty, Mech. Eng. Dept., Adana, Turkey
[3]Cukurova University, Faculty of Engineering and Architecture, Mech. Eng. Dept., Adana, Turkey
**E-mail address: nkurtulmus@adanabtu.edu.tr*
Orcid id: 0000-0002-8896-4079, 0000-0002-5339-6120, 0000-0003-0671-0890
Manuscript Received 06 October 2017, Accepted 30 October 2017

systems driven by waste heat from exhaust gas for air-conditioning vehicle cabins. They all confirmed the feasibility of the VAR system application.

Kilic and Kaynaklı [13] conducted a second law-based thermodynamic analysis of a VAR system using water-LiBr as the working fluid pair. They found that the highest rate of exergy loss at the generator corresponds to the rate of 45.68% of total exergy loss, and the lowest rate of exergy loss occurs at the pump and corresponds to the rate of 0.0034% of total exergy loss. Effects of varying the generator temperature on the exergy loss rate of each component and on the exergy efficiency of the VAR system were investigated. Şencan et al. [14] performed studies on the exergy analysis of a single-effect VAR system using water-LiBr solution. They found that the highest exergy loss occurs through the absorber and the lowest exergy loss occurs through the evaporator. Talbi and Agnew [15] also conducted an exergy analysis on a single-effect VAR system using water-LiBr solution. Gomri [16] made a comparison between single-effect and double-effect VAR systems in terms of the second law of thermodynamics. The obtained results reveal that the maximum COP of the single-effect VAR system is 0.79 and that the maximum COP of the double-effect VAR system is 1.42. In addition, the maximum exergy efficiency of the single-effect VAR system is about 23.2%, whereas the maximum exergy efficiency of the double-effect VAR system is approximately 25.1%. Energy and exergy analyses were conducted by Kaynakli et al. [17] on the double-effect VAR system to determine the effects of heat source types. They chose three types of heat sources, including hot air, steam, and hot water, to drive the system. Their results reported that the maximum exergy destruction occurs through the double-effect VAR system when hot air is used as the heat source. A few of the researchers analyzed the VAR system on an hourly basis of cooling load and solar power for air-conditioning applications. Another research was conducted by Arora et al. [18] on double-effect VAR system. An exergy analysis of a solar-assisted VAR system was performed by Onan et al. [19].

In this study, energy and exergy analyses are conducted for an application of the VAR system for air-conditioning an intercity bus cabin with atmospheric data such as ambient temperature, solar radiation, and relative humidity on an hourly basis. The second objective is to investigate the effects of operating and environmental parameters on the system performance and exergy destruction of the system. Therefore, the advantages of VAR system application for air-conditioning purpose for an intercity bus cabin is presented at different conditions in terms of fuel saving, emissions and weight. To perform the analysis, components of a VAR system using water-LiBr solution as the working fluid are investigated in detail with respect to the variation of ambient parameters.

SYSTEM DESCRIPTIONS

Vapor Absorption Refrigeration System

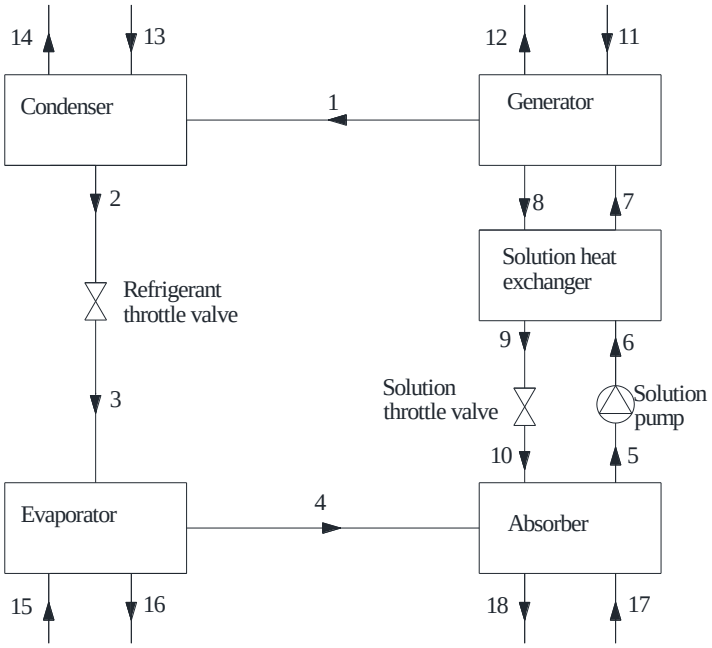

Figure 1. Schematic illustration of the vapor absorption refrigeration system

As seen in Figure 1, the single-effect VAR system consists of the evaporator, condenser, generator, absorber, solution heat exchanger, solution pump, solution throttle valve, and refrigerant throttle valve. The generator, solution heat exchanger, and condenser operate at high pressure, and the evaporator and absorber operate at low pressure. The generator receives heat from exhaust gas. The absorber and condenser are cooled with ambient air and the evaporator takes heat to provide refrigeration.

Operating Conditions of the VAR System

In the modeled system, the generator of the VAR system is coupled with the exhaust system of the intercity bus to utilize waste heat of exhaust gas received from the 6-cylinder, 4-stroke turbocharged diesel engine that drives the bus. The data shown in Table 1 are taken from Yilmaz [20] and Shu et al. [21]. The gas mixture method [21] is applied to determine the exhaust gas properties, including specific heat, enthalpy, and entropy. For example, enthalpy of exhaust gas is calculated as follows and X, is the mass fraction of each individual gas in the exhaust gas.

$$h_{exgas} = X_{CO_2} h_{CO_2} + X_{O_2} h_{O_2} + X_{H_2O} h_{H_2O} + X_{N_2} h_{N_2} \quad (1)$$

Considering the highest and lowest ambient temperatures (because ambient temperature determines the condenser outlet temperature, so does the generator pressure) in terms of the VAR system performance, the generator temperature is chosen as 110 ºC. The exhaust gas mass composition (CO_2, N_2, O_2, H_2O) for different engine loads is shown in Table 1 [21].

Table 1. Data for the 6-cylinder, 4-stroke turbocharged diesel engine [20, 21]

Engine load (%)	Exhaust gas temperature (ºC)	Exhaust gas mass flow rate (kg/h)	Engine power output (kW)	Engine efficiency (%)	CO_2 (%)	N_2 (%)	O_2 (%)	H_2O (%)
50	420	610.91	117.7	41.72	12.4	73.8	9	4.8
75	474	804.43	176.2	42.15	13.9	73.4	7.2	5.5
90	498	930.81	211.6	41.89	14.5	73.2	6.6	5.7
100	519	990.79	235.8	41.81	15.2	73	5.8	6

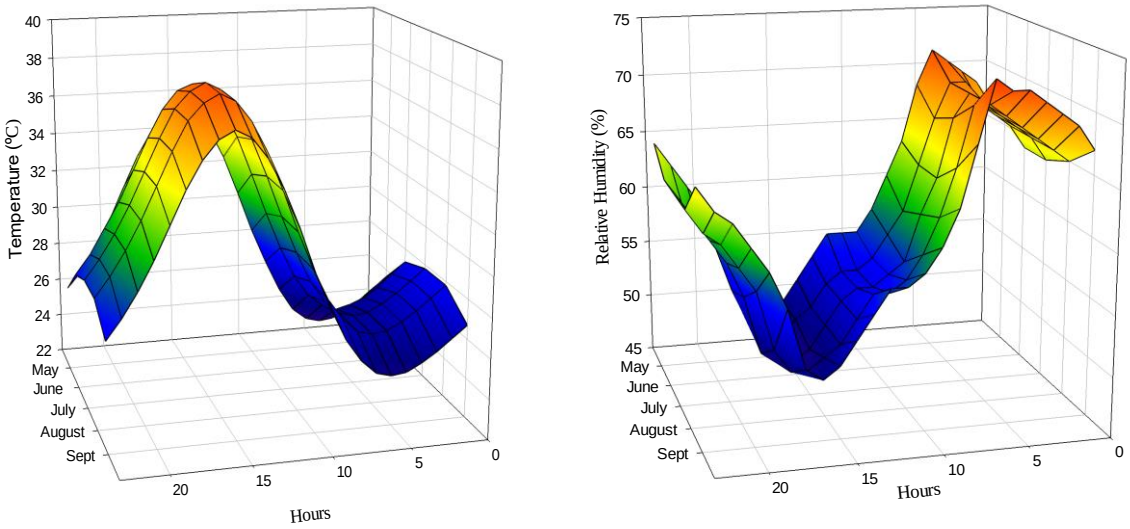

Figure 2. (a) Hourly environmental temperature distributions, (b) Hourly relative humidity distributions

The evaporator is used in a TS 45 type intercity bus cabin belonging to TEMSA Bus Company to meet the comfort cooling load calculated for Adana province in Turkey. For performing energy and exergy analyses,

temperature and humidity in the bus cabin are taken as 24 ºC and 50%, respectively. The other main components, such as the condenser and absorber, are integrated into the bus appropriately, and they release heat to the medium of outdoor air. Temperatures of the condenser and absorber are determined to be T_A+14 ºC [22, 23]. A simulation was prepared using Engineering Equation Solver (EES) software [24] for applying the energy and exergy analyses of the single-effect VAR system. In the analyses, the properties of water/steam and the enthalpy of water-LiBr were obtained from the EES library. The density and specific heat of water-LiBr were obtained from Florides et al. [25] and the entropy of water-LiBr was obtained from Chua et al. [26].

Hourly environmental temperature and the relative humidity values taken from the Turkish State Meteorological Service are shown in Figures 2(a) and 2(b), respectively. As is shown, the environmental temperature reaches a maximum of 38 ºC at 3 p.m. in July and August and a minimum 23.4 ºC at 5 a.m. in May. Maximum relative humidity is 73% at 6 a.m. in September, and the minimum is 48% at 4 p.m. in June and at 5 p.m. in July.

Assumptions

The following assumptions were made [16, 17]:

- All system components are at steady-state conditions.
- Refrigerant leaving the condenser is saturated water at condenser pressure, and refrigerant leaving the evaporator is saturated vapor at evaporator pressure.
- Condenser pressure is equal to generator pressure, and evaporator pressure is equal to absorber pressure.
- There is no pressure drop in the heat exchangers or piping systems.
- There are no heat losses or gains in the various components and piping systems.
- Temperature and pressure at the reference state are 298 K and 101.325 kPa, respectively. Enthalpy and entropy of the working fluid at the reference state used for calculating the exergy of the VAR system are equal to the values of water at an environmental temperature and pressure of 25 ºC and 101.325 kPa, respectively.
- The kinetic, chemical, and potential exergy of all streams of the VAR system are negligible.
- The solution pump efficiency is 0.9.
- The specific humidity is constant for heat exchangers in the VAR system.

Thermodynamic Analysis of the VAR System

Mass balance and energy conversion methods are implemented to determine and optimize the capacity of the components and the COP value of the VAR system. These methods provide any necessary information about the irreversibility of the components of the VAR system. Cengel and Boles [27] reported that entropy production and exergy destruction analyses could be utilized to set up principles for the performance of engineering systems such as absorbers, generators, condensers, and evaporators. Entropy production can be used as a quantitative degree of irreversibilities related to the processes. The performance of engineering systems is decayed by the existence of irreversibility during processes. An increase in irreversibilities increases entropy production. There is no irreversibility in a reversible process, but reversible processes, in fact, do not occur in nature. In addition, reversible processes can be considered to be theoretical limits for the related irreversible processes. For that reason, exergy analysis is substantially important for the performance of a vapor absorption refrigeration system [19, 21].

Exergy is defined as the maximum work potential of a matter or a form of energy with respect to its reference environment [13].

The mass balance equations for the system components are as follows:

$$\sum \dot{m}_i = \sum \dot{m}_e \tag{2}$$

$$\sum \dot{m}_i X_i = \sum \dot{m}_e X_e \tag{3}$$

The flow ratio, f, is a parameter that helps to calculate the heat capacities of the components of VAR system. The LiBr balance of the generator is used to obtain the flow ratio, which is defined as the ratio of the strong solution of mass flow rate, $\dot{m}_{s,}$ to the refrigerant mass flow rate, $\dot{m}_r$.

$$f = \frac{\dot{m}_s}{\dot{m}_r} = \frac{X_7}{X_8 - X_7} \tag{4}$$

General energy and exergy balance equations are given as follows [23]:

$$E_i = E_o \tag{5}$$

$$\dot{E}x_i - \dot{E}x_o = \dot{E}x_{dest} \tag{6}$$

$$\dot{E}x = \dot{m}(ex) \tag{7}$$

$$ex = h - h_0 - T_0(s - s_0) \tag{8}$$

Heat capacity, $\dot{Q}$, and exergy destructions, $\dot{E}x_{dest}$, obtained from energy and exergy balances of each of the components of the VAR system illustrated in Figure 1 can be expressed as follows [14, 15]:

$$q_{CO} = \frac{\dot{Q_{CO}}}{\dot{m}_1} = h_2 - h_1 \tag{9}$$

$$\dot{E}x_{dest,CO} = \dot{m}_1(ex_1 - ex_2) + \dot{m_{13}}(ex_{13} - ex_{14}) \tag{10}$$

$$q_{EV} = \frac{\dot{Q_{EV}}}{\dot{m}_1} = h_4 - h_3 \tag{11}$$

$$\dot{E}x_{dest,EV} = \dot{m}_3(ex_3 - ex_4) + \dot{m}_{15}(ex_{15} - ex_{16}) \tag{12}$$

$$q_{GE} = \frac{\dot{Q_{GE}}}{\dot{m}_1} = h_1 + fh_8 - (f+1)h_7 \tag{13}$$

$$\dot{E}x_{dest,GE} = \dot{m}_{11}(ex_{11} - ex_{12}) + \dot{m}_7 ex_7 - \dot{m}_8 ex_8 - \dot{m}_1 ex_1 \tag{14}$$

$$q_{AB} = \frac{\dot{Q_{AB}}}{\dot{m}_1} = (f+1)h_5 - h_4 - fh_{10} \tag{15}$$

$$\dot{E}x_{dest,AB} = \dot{m}_{17}(ex_{17} - ex_{18}) + \dot{m}_4 ex_4 + \dot{m}_{10} ex_{10} - \dot{m}_5 ex_5 \tag{16}$$

$$q_{she} = \frac{\dot{Q}_{she}}{\dot{m}_1} = f(h_8 - h_9) = (f+1)(h_7 - h_6) \tag{17}$$

$$\dot{E}x_{dest,SHE} = \dot{m}_8(ex_8 - ex_9) + \dot{m}_5(ex_6 - ex_7) \tag{18}$$

$$\dot{E}x_{dest,rtv} = \dot{m}_1 T_0(s_3 - s_2) \tag{19}$$

$$\dot{W}_p = \dot{m}_5(h_6 - h_5) = \frac{\dot{m}_5 \vartheta_s (P_{CO} - P_{EV})}{n_p} \quad (20)$$

$$\dot{Ex}_{dest,p} = \dot{m}_5(ex_5 - ex_6) + \dot{W}_p \quad (21)$$

$$\dot{Ex}_{dest,tot} = \sum_{j=1}^{N} Ex_{dest,j} \quad (22)$$

$$COP_{VAR} = \frac{\dot{Q_{EV}}}{\dot{Q_{GE}} + W_p} \quad (23)$$

RESULTS AND DISCUSSION

To validate the present model, the simulation results were compared with the previous works available in the literature. The comparative heat capacities, $\dot{Q}$, coefficients of performance, COP, and exergy destructions, $\dot{Ex}_{dest}$, of the VAR system are presented in Table 2. For validations, the following input parameters were used: T_{GE} = 87.8 °C, T_{EV} = 7.2 °C, T_{CO} = T_{AB} = 37.8 °C, the effectiveness of solution heat exchanger, ϵ = 0.7, and refrigerant mass flow rate, $\dot{m}_r$ = 1 kg/s. As seen, the results obtained from the present simulation are in good agreement with the literature.

Table 2. Comparison of the analytical results with data given in the literature

	Anand and Kumar [28]	**Arora and Kaushik [29]**	**Present study**
$\dot{Q}_{GE}$ **(kW)**	3073.11	3095.698	3078.547
$\dot{Q}_{AB}$ **(kW)**	2922.39	2945.269	2932.376
$\dot{Q}_{CO}$ **(kW)**	2507.89	2505.91	2505.910
$\dot{Q}_{EV}$ **(kW)**	2357.17	2355.45	2355.450
$\dot{Q}_{SHE}$ **(kW)**	523.25	518.717	529.465
W_P **(kW)**	-	0.03143	0.03431
COP	0.76703	0.7609	0.7651
$Ex_{dest,GE}$ **(kW)**	-	55.568	54.639
$Ex_{dest,AB}$ **(kW)**	-	70.478	67.420
$Ex_{dest,CO}$ **(kW)**	-	6.606	6.606
$Ex_{dest,EV}$ **(kW)**	-	86.275	87.524
$Ex_{dest,SHE}$ **(kW)**	-	25.081	26.608
$Ex_{dest,RTV}$ **(kW)**	-	6.936	6.936
$Ex_{dest,TOT}$ **(kW)**	-	250.967	249.733
Ex_{INPUT} **(kW)**		538.637	535.622
Ex_{OUTPUT} **(kW)**		63.277	62.028
η		0.1175	0.1158

The heat capacity of evaporator, $\dot{Q}_{EV}$, is equal to the hourly comfort cooling load of the subject bus model. As seen in Figure 3(a), the minimum heat capacity of the evaporator, $\dot{Q}_{EV}$, is 13.17 kW at 6 a.m. in September, and the maximum heat capacity of the evaporator, $\dot{Q}_{EV}$, is 25.96 kW at 5 p.m. in July. As expected, the comfort cooling load at night hours is lower than in day hours. The trend of hourly exergy destruction, $\dot{Ex}_{dest,EV}$, values shown in Figure 3(b) is similar to that of the heat capacity of the evaporator. The highest exergy destruction, $\dot{Ex}_{dest,EV}$, occurring in the evaporator is 0.9631 kW at 5 p.m. in July, and the lowest exergy destruction, $\dot{Ex}_{dest,EV}$, occurring in the evaporator is 0.4885 kW at 6 a.m. in September.

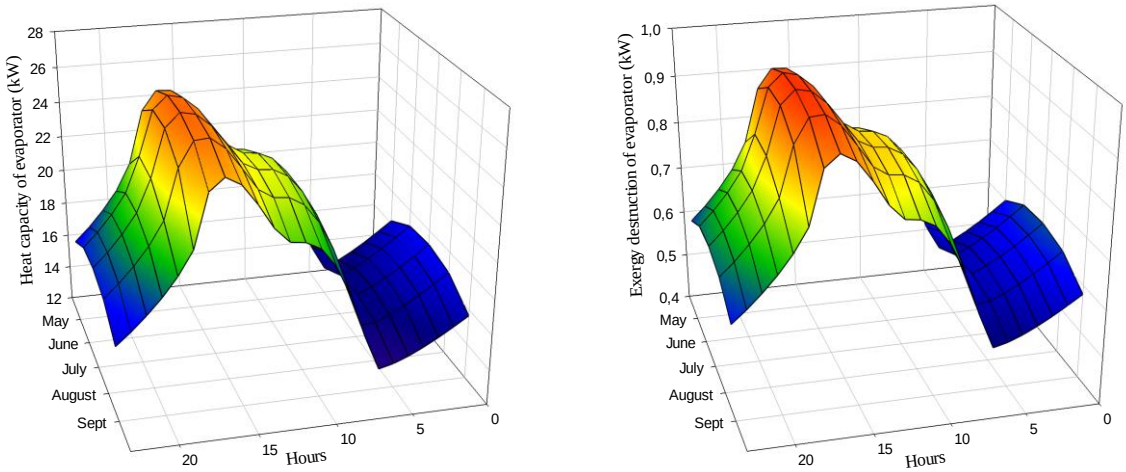

(a) (b)

Figure 3. (a) Hourly variation of heat capacity for the evaporator, (b) hourly variation of exergy destruction for the evaporator

The COP variation of the VAR system is shown in Figure 4(a). The maximum COP value of the VAR system is 0.778 at 5 a.m. in May, and the corresponding outdoor temperature, T_o, is 23.4 ºC. The minimum COP value of the VAR system is 0.6628 at 3 p.m. in July and August, and the corresponding outdoor temperature is 38 ºC. Figure 4(b) shows the hourly variation of total exergy destruction, $\dot{E}x_{dest,TOT}$, for the VAR system. The lowest total exergy destruction, $\dot{E}x_{dest,TOT}$ value is 8.69 kW at 6 a.m. in September and the corresponding outdoor temperature, T_o, and relative humidity, RH are 24.7 ºC, 73%, respectively. The highest total exergy destruction, $\dot{E}x_{dest,TOT}$ value is 15.25 kW at 4 p.m. in July and the corresponding outdoor temperature, T_o, and the relative humidity, RH, are 37.6 ºC, 48%, respectively. The results indicate that the COP of the system decays in day hours and rises at night. On the other hand, the total exergy destruction increases in day hours and decays at night.

To present the benefits of a VAR system driven by exhaust gas waste heat received from the engine, the results for using a conventional VCR system driven by the engine by a belt drive should be studied for the purpose of comparison. The COP variation of the VCR system and the compressor (which is the main energy consumer in the basic VCR system) load variations on an hourly basis during the cooling season are presented in Figures 4(c) and 4(d). The temperatures of the evaporator and condenser for the VCR and VAR systems are assumed to be equal. The VCR system is assumed for the calculations to use R134a refrigerant as a working fluid. The calculated results reveal that the maximum coefficient of performance, COP, is equal to 3.9 and that the minimum COP is equal to 2.67, based on the outdoor temperatures. A similar trend is obtained for the VAR system. It is worth mentioning that the compressor of the VCR system consumes considerable energy, as seen in Figure 4(d). Specifically, this power input varies between 3.84 kW and 9.57 kW. When the compressor load is at maximum, it consumes approximately 9% of the power received from the engine when the engine works 50% load. Figure 4(e) shows the hourly variation of fuel consumption of the VCR system. First, the specific fuel consumption by the engine is calculated as follows [30]:

$$BSFC = \frac{1}{n * 0.0119531} \tag{24}$$

At equation (24), lower heating value of diesel fuel is taken as 0.0119531 kWh/g [30] and engine efficiency is taken from Table 1.

Then the fuel consumption is calculated by using brake-specific fuel consumption (BSFC) and the energy required by the compressor [31]. As can be seen from the figure, the fuel consumption of the compressor varies between 698.56 g/h and 1919.31 g/h. If the air conditioning system works through the cooling season, the compressor consumes fuel at the rate of 4,489 kg/year. This value is crucial because it releases emissions after

the combustion process and because the consumption of fossil fuel causes vitally important environmental problems. The hourly variation of CO_2 emission caused by the VCR system is shown In Figure 4(g). It varies between 2,242.08 g/h and 6,160.16 g/h during the cooling season. If the air conditioning system works through the entire cooling season, the total of released CO_2 emission is calculated as 14,407.05 kg/year.

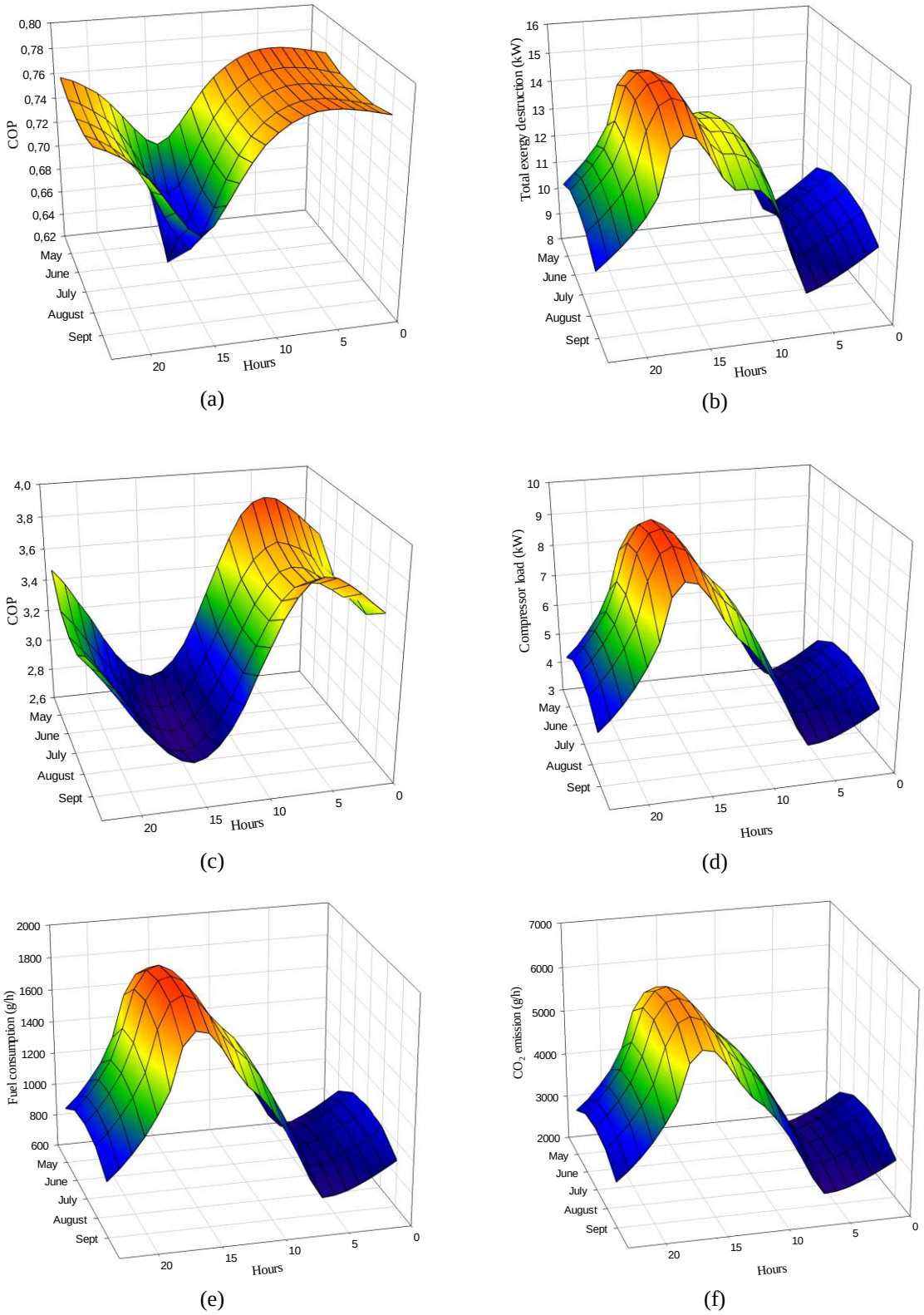

Figure 4. (a) Hourly variation of COP of the VAR system, (b) hourly variation of total exergy destruction of the VAR system, (c) hourly variation of COP of the VCR system, (d) hourly variation of compressor load of the VCR system, (e) hourly variation of fuel consumption of the VCR system, (f) hourly variation of CO_2

emission of the VCR system

The fuel consumption values and CO_2 emission quantities are calculated for the engine under 50% load. The weight issue should also be considered when the use of a VAR system driven by exhaust gas is investigated for an intercity bus. So, the VAR system components are designed and constructed by using heat and mass transfer calculations. The heat transfer capacity of the main components of the VAR system is calculated as follows;

$$\dot{Q} = U \cdot A \cdot \Delta T_m \tag{25}$$

The overall heat transfer coefficient, U can be determined as shown below;

$$\frac{1}{U \cdot A} = \sum R_{conv} + \sum R_f + \sum R_{cond} \tag{26}$$

where the thermal resistance is represented by R.

$$\Delta T_m = \frac{\Delta T_1 - \Delta T_2}{ln(\frac{\Delta T_1}{\Delta T_2})} \tag{27}$$

Here, ΔT_1 and ΔT_2 are presented as $\Delta T_1 = T_{ho} - T_{ci}$ and $\Delta T_2 = T_{hi} - T_{co}$. All of the components, except solution heat exchanger, are designed to be circular finned tube heat exchanger. Circular fins are suited at the outside of the tubes. While air and exhaust gas passes the outside of the finned tubes, the working fluid passes inside of the smooth tubes. For the calculation of the outside heat transfer coefficient, h_o of heat exchangers, the Young and Brigs [32] equation is used which is stated below:

$$Nu = 0.134 Re^{0.681} Pr^{\frac{1}{3}} (\frac{l}{b})^{0.2} (\frac{l}{\tau})^{0.1134} \tag{28}$$

The inner side heat transfer coefficient of heat exchangers such as condensing, evaporating, film convection and mass transfer coefficient is calculated by guidelines of Florides [28] and Garousi Farshi et al. [33]. The solution heat exchanger is designed as a double pipe heat exchanger and the equation stated below was used [33]:

$$Nu = 0.023 Re^{0.8} Pr^{n} \tag{29}$$

Assumptions and calculated results to be applied for the present system are summarized in Table 3. When taking the assumptions at Table 4, the point that highest exergy destruction occurs is considered, see table 5. As seen in Table 4, the total mass of the components of VAR system is 349.14kg. Currently, the Temsa TS45 model intercity bus uses ES348 model VCR system belonging SAFKAR Company. The unit provides 32 kW cooling power capacity, and its mass with the piping system and compressor is approximately 200 kg. It is estimated that a 10% increase in the mass of the vehicle decreases the fuel economy by about 7% [34]. It can be seen that, considering TS45 intercity bus's gross vehicle mass rating of 23,360 kg [35]. And the calculated maximum capacity of the evaporator shown in Figure 3a, the mass increment of the present VAR system driven by exhaust gas, compared to that of the conventional VCR system for air conditioning purposes, may be ignored in terms of fuel consumption.

After examination of the parameters related to the conventional VCR system, computation of those parameters that affect the VAR system performance and exergy destruction at specified hours throughout the cooling season becomes significant. For example, the highest total exergy destruction for the present system occurs at 4 p.m. in July when the temperature and the relative humidity are 37.6 ºC and 48%, respectively. Figures 5-9 are prepared using the parameters given in Table 3, and the effectiveness of the solution heat exchanger, ϵ, is taken as 0.7 in the analysis.

Table 3. Assumptions and calculated values of the VAR system

States	Substance	T (°C)	P (kPa)	X (%)	m (kg/s)	h (kj/kg)	s (kj/kgK)
1	Superheated vapor	110	13.36	-	0.0112	2705.65	8.363
2	Saturated water	51.6	13.36	-	0.0112	216.02	0.7244
3	Water-vapor	10	1.23	-	0.0112	216.02	0.7656
4	Saturated vapor	10	1.23	-	0.0112	2518.89	8.899
5	Water-LiBr	51.6	1.23	61.2	0.1914	144.31	0.2794
6	Water-LiBr	51.6	13.36	61.2	0.1914	144.31	0.2794
7	Water-LiBr	88.14	13.36	61.2	0.1914	213.57	0.4798
8	Water-LiBr	110	13.36	65	0.1802	271.15	0.556
9	Water-LiBr	68.93	13.36	65	0.1802	197.59	0.3554
10	Water-LiBr	68.93	1.23	65	0.1802	197.59	0.3554
11	Exhaust gas	420	101.3	-	0.1697	-1323.93	7.6425
12	Exhaust gas	217.5	101.3		0.1697	-1549.52	7.2582
13	Outdoor air	37.6	101.3	-	3.823	88.54	5.9165
14	Outdoor air	44.6	101.3		3.823	95.84	5.9398
15	Indoor air	24	101.3		3.6	47.82	5.779
16	Indoor air	17	101.3		3.6	40.66	5.7546
17	Outdoor air	37.6	101.3		4.963	88.54	5.9165
18	Outdoor air	44.6	101.3		4.963	95.84	5.9398

Table4. The parameters of components of VAR system

	Absorber	Generator	Condenser	Evaporator	Sol. heat ex.
$\dot{Q}$ (kW)	35.56	37.6	28	25.95	11.19
d_i (mm)	23.4	23.4	23.4	23.4	Inner tube: 18 Outer tube:23.6
d_o (mm)	25.4	25.4	25.4	25.4	Inner tube: 21.3 Outer tube:26.9
b (mm)	10	10	10	10	-
l (mm)	2.75	2.75	2.75	2.75	-
τ (mm)	0.5	0.5	0.5	0.5	-
Fin area(m^2)	87.09	2.05	39.45	55.96	-
Tube array	3X28	2X4	2X24	3X23	-
L (mm)	1515	374	1201	1185	Total length: 21700
P_t (mm)	44	40	44	40	-
U ($W/m^{2o}C$)	36.21	84.76	62.97	41.11	380.85
ΔT_m	10.1	194.05	10.1	10.1	20.25
Components mass (kg)	145.79	3.38	66.04	93.76	40.17

Table 5 shows that the generator has the highest heat capacity, $\dot{Q}$, and exergy destruction, $\dot{E}x_{dest}$, values. The smallest amount of heat capacity and exergy destruction occurs in the solution pump.

Table 5. Heat capacity and exergy destruction of each unit of the VAR system, COP = 0.67

Parameter	Value (kW)
Evaporator heat capacity	25.79
Condenser heat capacity	27.89
Generator heat capacity	38.29
Absorber heat capacity	36.20
Solution heat exchanger	13.25
Pump power	0.0015
Exergy destruction of evaporator	0.957
Exergy destruction of condenser	0.996
Exergy destruction of generator	10.97
Exergy destruction of absorber	1.54
Exergy destruction of sol. heat ex.	0.699
Exergy destruction of ref. tho. valve	0.1376
Exergy destruction of pump	0.00136
Total exergy destruction	15.25

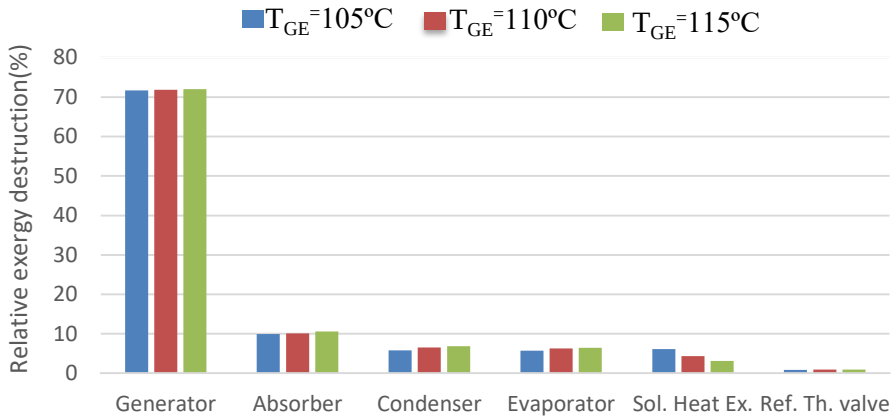

Figure 5. Relative exergy destruction of the VAR components (%)

Figure 5 presents the rate of relative exergy destruction of the VAR system components. To show the effects of generator temperature, T_{GE}, on the relative exergy destruction of the VAR system components, three different generator temperatures are examined. Because of the large heat capacity and temperature differences between streams, the highest relative exergy destruction occurs through the generator. Increasing the generator temperature upgrades the relative exergy destruction of the generator, absorber, condenser, evaporator, and refrigerant throttle valves because it decreases the total exergy destruction of the VAR system. The highest rate of relative exergy destruction of the generator is 72.04% at T_{GE} = 115 ºC, and the lowest rate of relative exergy destruction of the generator is 71.67% at T_{GE} = 105 ºC. The absorber has the second highest rate of relative exergy destruction, which is 10.6% at T_{GE} = 115 ºC, but this rate decreases to a value of 9.93% at T_{GE} = 105 ºC. The condenser and evaporator have approximately equal exergy destruction, which corresponds to 6.5% at T_{GE} = 115 ºC. The smallest rate of relative exergy destruction occurs at the refrigerant throttle valve, and that is 0.93% at T_{GE} = 115 ºC. Here the exergy destruction of the solution pump is ignored.

Figure 6 shows the change of total exergy destruction, $\dot{E}x_{dest,TOT}$, and exergy destruction of generator, $\dot{E}x_{dest,GE}$, with generator temperature, T_{GE}. The variation of parameters is investigated for three

different (source) temperatures of waste heat of exhaust gas, $T_{S,}$ including 410 ºC, 420 ºC, and 430 ºC. The exergy destruction of the generator, $\dot{E}x_{dest,GE}$, tends to decrease with increasing generator temperature, T_{GE}, and decreasing source temperature, T_S. When the generator temperature increases, although the temperature of the weak solution at the generator inlet increases, the exergy of it decreases because of decreasing flow ratio, f. Since the change rate of exergy at the generator inlet is higher than that of the other streams, the exergy destruction of the generator, $\dot{E}x_{dest,GE}$, decreases. Also, an increase in the exhaust gas outlet temperature, $T_{o,exgas}$, makes a contribution to decrease the exergy destruction value of the generator. While the maximum exergy destruction of generator, $\dot{E}x_{dest,GE}$ is 13 kW at T_S= 430 ºC and T_{GE}=104 ºC, which corresponds to the rate of 21% reduction which represents a minimum value that is 10.18 kW at T_S = 410 ºC and T_{GE} = 118 ºC. On the other hand, the total exergy destruction, $\dot{E}x_{dest,TOT}$, of the VAR system has a maximum value of 18.08 kW, which occurs at T_S = 430 ºC and T_{GE} = 104 ºC. However, the total exergy destruction, $\dot{E}x_{dest,TOT}$, decreases with increasing generator temperature, T_{GE}, and with decreasing source temperature, T_S. Finally, it can be stated that the minimum total exergy destruction, $\dot{E}x_{dest,TOT}$, occurs with a minimum value of 14.3 kW at T_S = 410 ºC and T_{GE} = 118 ºC.

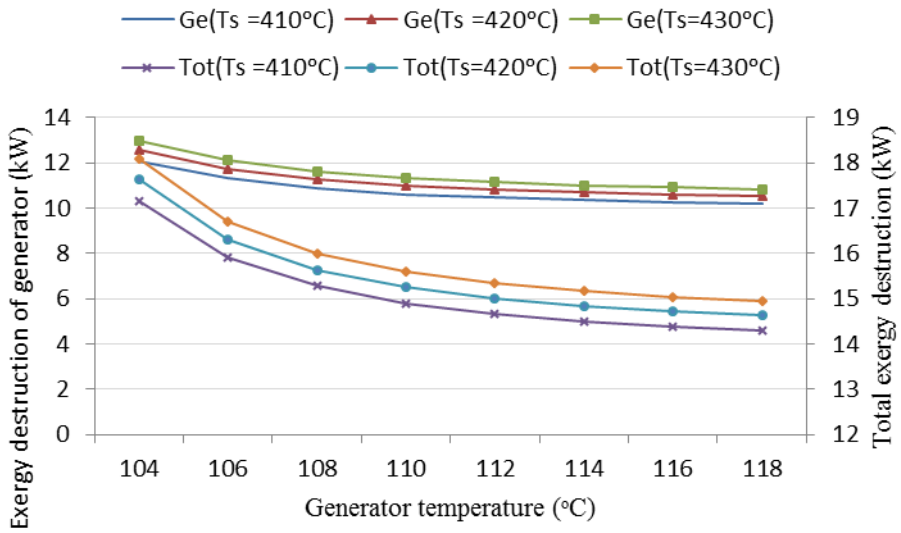

Figure 6. Variation of total exergy destruction and exergy destruction of the generator with increasing generator temperature

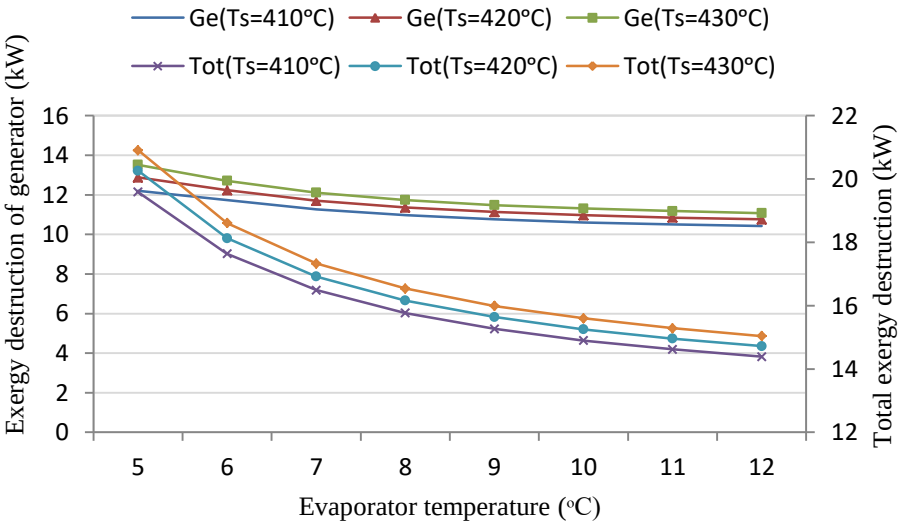

Figure 7. Variations of total exergy destruction of the VAR system and exergy destruction of the generator based on variation of evaporator temperatures

The effect of evaporator temperature, T_{EV}, on the variation of total exergy destruction, $\dot{E}x_{dest,TOT}$, of the system and exergy destruction of the generator, $\dot{E}x_{dest,GE}$, is presented in Figure 7. As illustrated in the figure, the exergy destruction of the generator, $\dot{E}x_{dest,GE}$, declines about 18% with increasing the evaporator temperature, T_{EV}, but with decreasing the source temperature, T_S. Upgrading the evaporator temperature provides a lower generator heat load, and exhaust gas outlet temperature rises. That increases the exergy value of exhaust gas at the generator outlet, leading the exergy destruction of generator, $\dot{E}x_{dest,GE}$, to decrease. The total exergy destruction, $\dot{E}x_{dest,TOT}$, of the VAR system decays about 31% when the evaporator temperature, T_{EV}, is increased but the source temperature, T_S, is decreased.

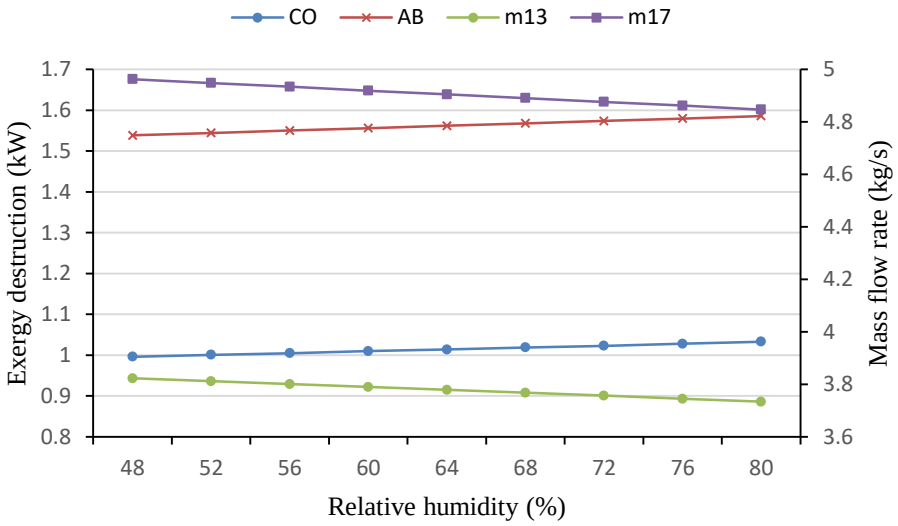

Figure 8. The effect of relative humidity on the absorber and condenser parameters

Figure 8 demonstrates changes of exergy destruction of the absorber and condenser and required mass flow rate to release heat to the ambient with changes in relative humidity, RH. Because the absorber and condenser are cooled by ambient air, changes of relative humidity, RH, of the ambient air influences only these components of the VAR system. In summary, variations of exergy destruction and required mass flow rate of condenser, $\dot{m}_{13}$, and absorber, $\dot{m}_{17}$, against relative humidity, RH, are not rapid.

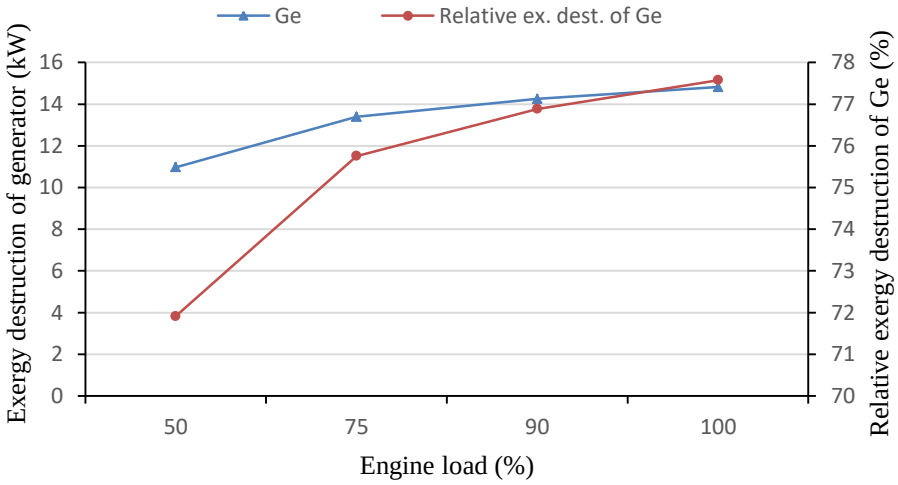

Figure 9. The effect of engine load variation on the parameters of the generator

The variations of the exergy destruction of the generator, $\dot{E}x_{dest,GE}$, and the relative exergy destruction of the generator, which are valuable parameters, are shown in Figure 9 on the basis of the data given in Tables 1,4 and 5. As seen in the figure, exergy destruction of the generator, $\dot{E}x_{dest,GE}$, as well as the relative exergy destruction of the generator, increases with increasing engine load. The lowest exergy destruction of the generator, $\dot{E}x_{dest,GE}$, is 10.97 kW at an engine load rate of 50%. On the other hand, it is clearly seen that the maximum exergy destruction occurs with a value of 14.82 kW when the engine is run at a 100% load rate. The slope of the relative exergy destruction curve of the generator decreases sharply when the engine is run at a 75% load rate. In conclusion, the lowest relative exergy destruction rate of the generator is 71.91% at the engine load rate of 50%, but it increases to a maximum value of 77.57% at the engine load of 100%.

CONCLUSION

The Vapor Absorption Refrigeration system driven by waste heat of the exhaust gas received from the internal combustion engine is investigated for cabin air-conditioning purposes on an intercity bus in cooling season. To perform the energy and exergy analyses, a single-effect VAR system using water-LiBr solution is selected as working solution pair. Effects of environmental conditions and operating parameters on the system performance, exergy destruction, and heat capacities of various components of the VAR system are presented and discussed. The following conclusions can be drawn from the present research:

- During cooling season, the lowest heat capacity of the evaporator, which is 13.17 kW, is obtained at 6 a.m. in September, and the highest heat capacity of the evaporator, 25.96 kW, is obtained at 5 p.m. in July.
- The maximum COP of the VAR system is calculated as 0.778 at 5 a.m. in May, and the minimum COP is calculated as 0.6628 at 3 p.m. in July and August.
- Air-conditioning an intercity bus in cooling season by a VAR system driven by exhaust gas waste heat is possible, even at an engine load rate of 50%.
- Approximately 4,489 kg/year of fuel can be saved by using the VAR system driven by an exhaust gas waste heat in an intercity bus during the cooling season. Thus, it prevents 14,407 kg/year of CO_2 emissions released to the environment.
- The minimum total exergy destruction is obtained as 8.69 kW at 6 a.m. in September; conversely, the maximum total exergy destruction is determined to be 15.25 kW at 4 p.m. in July.
- The relative exergy destruction of each components of the VAR system, except for the solution heat exchanger, tends to rise with rising generator temperature. The generator has the highest relative exergy destruction, which correspond to the rate of 71.93% at T_{GE} = 110 ºC.
- Finally, it is found that the total exergy destruction may be reduced by about 30% by increasing generator and evaporator temperatures and decreasing exhaust gas inlet temperature.

NOMENCLATURE:

A	Area (m^2)
b	fin height
BSFC	Brake specific fuel consumption (g/kWh)
COP	Coefficient of Performance
c_p	Specific heat (J/kgK)
d	tube diameter (m)
d_h	hydraulic diameter (m)
Ė	Energy (kW)
Ėx	Exergy (kW)
ex	Specific exergy (kj/kg)
f	flow ratio
h	enthalpy (kj/kg), convection coefficient (W/m^2K)
k	conduction coefficient (W/m^2K)
l	fin spacing
L	length of one tube

Libr	lithium bromide
$\dot{m}$	Mass flow rate (kg/s)
n	engine efficiency
N	total number of components in system
Nu	Nusselt number, ($h*d_h/k$)
P	Pressure (kPa), pitch
Pr	Prandlt number, ($\mu*c_p/k$)
RH	relative humidity (%)
Re	Reynolds number ($u*d_h/v$)
$\dot{Q}$	heat capacity (kW)
q	specific heat capacity (kj/kg)
s	entropy (kj/kg/K)
Sept	September
T	Temperature
ΔT	Logarithmic temperature difference (ºC)
U	Overall heat transfer coefficient (W/m^2 ºC), velocity (m/s)
v	kinematic viscosity (m^2/s)
VAR	Vapor Absorption Refrigeration
VCR	Vapor Compression Refrigeration
W	Power (kW)
X	mass fraction
A	Ambient
AB	Absorber
c	cold fluid
CO	Condenser
cond	conduction
conv	convection
dest	destruction
e	exit
f	fouling
EV	Evaporator
exgas	Exhaust gas
GE	Generator
h	hot fluid
i	In, inlet, inner
j	number of components
m	mean
o	Out, outlet, outer
p	Pump
r	refrigerant
rtv	Refrigerant throttle valve
s	solution, source
she	Solution heat exchanger
t	tube
Tot	total
1.2…	state points
0	reference state
ϵ	effectiveness
η	exergy efficiency; efficiency
μ	dynamic viscosity (kg/ms)
ϑ	specific volume (m^3/kg)
τ	fin thickness

Acknowledgements

The authors would like to thank to TEMSA Global for its contribution.

REFERENCES

[1] Hwang, Y. (2004). Potential energy benefits of integrated refrigeration system with microturbine and absorption chiller. International Journal of Refrigeration, 27(8), 816-829.

[2] www.johnsoncontrols.com. Application opportunities for absorption chillers. (accessed 17 January 2017)

[3] http://thermaxglobal.com. (accessed 17 January 2017)
[4] Horuz, I. (1998). A comparison between ammonia-water and water-lithium bromide solutions in vapor absorption refrigeration systems. International communications in heat and mass transfer, 25(5), 711-721.
[5] Little, A. B., & Garimella, S. (2011). Comparative assessment of alternative cycles for waste heat recovery and upgrade. Energy, 36(7), 4492-4504.
[6] Saidur, R., Rezaei, M., Muzammil, W. K., Hassan, M. H., Paria, S., & Hasanuzzaman, M. (2012). Technologies to recover exhaust heat from internal combustion engines. Renewable and sustainable energy reviews, 16(8), 5649-5659.
[7] Boatto, P., Boccaletti, C., Cerri, G., & Malvicino, C. (2000). Internal combustion engine waste heat potential for an automotive absorption system of air conditioning part 1: tests on the exhaust system of a spark-ignition engine. Proceedings of the Institution of Mechanical Engineers, Part D: Journal of Automobile Engineering, 214(8), 979-982.
[8] Manzela, A. A., Hanriot, S. M., Cabezas-Gómez, L., & Sodré, J. R. (2010). Using engine exhaust gas as energy source for an absorption refrigeration system. Applied energy, 87(4), 1141-1148.
[9] Koehler, J., Tegethoff, W. J., Westphalen, D., & Sonnekalb, M. (1997). Absorption refrigeration system for mobile applications utilizing exhaust gases. Heat and Mass Transfer, 32(5), 333-340.
[10] Horuz, I. (1999). Vapor absorption refrigeration in road transport vehicles. Journal of Energy Engineering, 125(2), 48-58.
[11] Boatto, P., Boccaletti, C., Cerri, G., & Malvicino, C. (2000). Internal combustion engine waste heat potential for an automotive absorption system of air conditioning part 1: tests on the exhaust system of a spark-ignition engine. Proceedings of the Institution of Mechanical Engineers, Part D: Journal of Automobile Engineering, 214(8), 979-982.
[12] Lambert, M. A., & Jones, B. J. (2006). Automotive adsorption air conditioner powered by exhaust heat. Part 1: conceptual and embodiment design. Proceedings of the Institution of Mechanical Engineers, Part D: Journal of Automobile Engineering, 220(7), 959-972.
[13] Kilic, M., & Kaynakli, O. (2007). Second law-based thermodynamic analysis of water-lithium bromide absorption refrigeration system. Energy, 32(8), 1505-1512.
[14] Şencan, A., Yakut, K. A., & Kalogirou, S. A. (2005). Exergy analysis of lithium bromide/water absorption systems. Renewable energy, 30(5), 645-657.
[15] Talbi, M. M., & Agnew, B. (2000). Exergy analysis: an absorption refrigerator using lithium bromide and water as the working fluids. Applied Thermal Engineering, 20(7), 619-630.
[16] Gomri, R. (2009). Second law comparison of single effect and double effect vapour absorption refrigeration systems. Energy Conversion and Management, 50(5), 1279-1287.
[17] Kaynakli, O., Saka, K., & Kaynakli, F. (2015). Energy and exergy analysis of a double effect absorption refrigeration system based on different heat sources. Energy Conversion and Management, 106, 21-30.
[18] Arora, A., Dixit, M., & Kaushik, S. C. (2016). Energy and exergy analysis of a double effect parallel flow LiBr/H2O absorption refrigeration system. Journal of Thermal Engineering, 2(1), 541-549.
[19] Onan, C., Ozkan, D. B., & Erdem, S. (2010). Exergy analysis of a solar assisted absorption cooling system on an hourly basis in villa applications. Energy, 35(12), 5277-5285.
[20] Yılmaz, A. (2015). Transcritical organic Rankine vapor compression refrigeration system for intercity bus air-conditioning using engine exhaust heat. Energy, 82, 1047-1056.
[21] Shu, G., Liu, L., Tian, H., Wei, H., & Xu, X. (2013). Performance comparison and working fluid analysis of subcritical and transcritical dual-loop organic Rankine cycle (DORC) used in engine waste heat recovery. Energy Conversion and Management, 74, 35-43.
[22] Yamankaradeniz, R., Horuz, I., Kaynakli, O., Coskun, S., & Yamankaradeniz, N. (2009). Refrigeration techniques and heat pump applications.
[23] Dincer, I., & Rosen, M. A. (2012). Exergy: energy, environment and sustainable development. Newnes.
[24] Klein, S. A. (2003). EES-engineering equation solver, professional version. F-chart software, Middleton, WI.
[25] Florides, G. A., Kalogirou, S. A., Tassou, S. A., & Wrobel, L. C. (2003). Design and construction of a LiBr–water absorption machine. Energy conversion and management, 44(15), 2483-2508.
[26] Chua, H. T., Toh, H. K., Malek, A., Ng, K. C., & Srinivasan, K. (2000). Improved thermodynamic property fields of LiBr–H2O solution. International Journal of Refrigeration, 23(6), 412-429.
[27] Y.A. Çengel, M. Boles, Thermodynamics: An Engineering Approach. New York: McGraw-Hill Series, 2011.
[28] Anand, D. K., & Kumar, B. (1987). Absorption machine irreversibility using new entropy calculations. Solar Energy, 39(3), 243-256.
[29] S.C. Kaushik, A. Arora, "Energy and exergy analysis of single effect and series flow double effect water–lithium bromide absorption refrigeration systems", International Journal of Refrigeration, 2009.

[30] Wikipedia, The free encyclopedia, https://en.wikipedia.org/wiki/Brake_specific_fuel_consumption. (accessed 17 January 2017)
[31] Hegar, M., Kolda, M., Kopecka, M., Rajtmajer, V., & Ryska, A. (2013). Bus HVAC energy consumption test method based on HVAC unit behavior. International Journal of Refrigeration, 36(4), 1254-1262.
[32] Robinson, K. K., & Briggs, D. E. (1966). Pressure drop of air flowing across triangular pitch banks of finned tubes. In Chem. Eng. Prog. Symp. Ser (Vol. 62, No. 64, pp. 177-184).
[33] Farshi, L. G., Mahmoudi, S. S., Rosen, M. A., Yari, M., & Amidpour, M. (2013). Exergoeconomic analysis of double effect absorption refrigeration systems. Energy Conversion and Management, 65, 13-25.
[34] Ghassemieh, E. (2011). Materials in automotive application, state of the art and prospects. In New trends and developments in automotive industry. InTechOpen..
[35] Temsa TS45 Broshure, http://chbussales.com/wp-content/uploads/2015/01/2015-TS-45-Brochure_Online.pdf. (accessed 17 January 2017)